Available online at www.sciencedirect.com
SCIENCE DIRECT
Polymer 46 (2005) 8275–8285
polymer
www.elsevier.com/locate/polymer

Morphological and structural characterization of polypropylene based nanocomposites

Edmondo Maria Benetti[a], Valerio Causin[a,*], Carla Marega[a], Antonio Marigo[a], Giuseppe Ferrara[b], Angelo Ferraro[b], Marco Consalvi[b], Fabiana Fantinel[b]

[a]*Dipartimento di Scienze Chimiche and INSTM Research Unit, Università di Padova, via Marzolo 1, 35131 Padova, Italy*
[b]*Basell Poliolefine Italia SpA, Centro Ricerche 'Giulio Natta', P.le Donegani 12, 44100 Ferrara, Italy*

Received 18 March 2005; received in revised form 17 May 2005; accepted 6 June 2005
Available online 20 July 2005

Abstract

Nanocomposites based on isotactic polypropylene and montmorillonite were studied, investigating the polymorphism of the polymer, and examining the interaction between polypropylene and silicate. Wide angle X-ray diffraction (WAXD) was used to study the crystallization of the matrix, particularly the influence of additives and processing. Small angle X-ray scattering (SAXS) was employed to assess the lamellar morphology, estimating how silicate dispersion could affect this factor. Interaction between polymer and clay was quantified from WAXD and SAXS profiles; by the position and shape of the clay basal peaks, two different degrees of interaction were identified, characterized by a different affinity between the constituents. Observation of the samples' morphology by transmission electron microscopy (TEM) confirmed the results of X-ray diffraction methods. A fitting procedure was applied to SAXS profiles and the dimensions of the clay stratifications were estimated. These results were successfully compared with those drawn by application of Scherrer equation on (001) WAXD peaks.

Keywords: Nanocomposites; Polypropylene; Small angle X-ray scattering

1. Introduction

Polymer based nanocomposites may offer a significant improvement in many physical and engineering properties with a very low filler loading. Among these properties are stiffness, strength, dimensional stability and permeability [1–5].

A large interfacial area per volume of particles is critical for the efficiency of a filler [6] and the technological potential of nanocomposites resides in the possibility of maximizing the extension of the interfacial region between matrix and filler.

Polymer–clay nanocomposites use smectite-type clays as fillers, such as hectorite, montmorillonite or synthetic mica, all minerals with a layered structure. The layers are characterized by a high aspect ratio as they have thicknesses of about 1 nm and diameters varying from 30 nm to several microns or more [7,8]. Hundreds or thousands of these layers are stacked in clay particles, kept together by weak van der Waals forces. The performance of polymer–clay nanocomposites strongly depends on the breaking-up of clay particles in the polymer matrix. As the degree of interaction between polymer and filler varies, three systems are generally found: clay sheets may remain stacked in structures called tactoids, as in the original mineral without any improvement compared to usual microcomposites with a low filler loading; polymer chains may penetrate into interlayer spacing, producing an intercalated system where clay layers are more separated; finally, an exfoliated structure could appear, with the single clay sheets delaminated and dispersed in the matrix. The latter system is the most desirable since nanometric dispersion of clay platelets ensures a maximization of the interfacial region between the filler and the polymer matrix, and a consequent improvement in reinforcement effect. If exfoliation occurs, the excellent mechanical properties [9–11] of the individual clay layers can be effectively exploited and the number of reinforcing components is dramatically increased, since each clay particle contains a very large number of clay sheets.

* Corresponding author. Tel.: +39 49 8275153; fax: +39 49 8275161.
E-mail address: valerio.causin@unipd.it (V. Causin).

0032-3861/$ - see front matter © 2005 Elsevier Ltd. All rights reserved.
doi:10.1016/j.polymer.2005.06.056

In the last 50 years, polypropylene (PP) has become one of the most widespread commodities, employed in the industry due to its low cost and good mechanical performance. The development of nanocomposites based on this polymer would thus be of critical importance for the industrial diffusion of such a novel class of materials. The preparation of PP-based nanocomposites has already been discussed in several publications [12–17] and presents some problems, the most important of which lies in the considerable difference in polarity between resin and clay. Pretreatment of both polymer and clay is, therefore, necessary. Clays are usually modified by cationic surfactants like organic ammonium salts or alkyl phosphonium [4] that make the clay surface more organophilic. As a consequence of this modification, clays are referred to as organoclays. PP's compatibility with organoclays is obtained by grafting polar functional groups such as maleic anhydride. Very promising results have been obtained using a mixture of PP, maleated polypropylene (PP-MA) and organoclay [18]. Only the addition of considerable amounts of PP-MA (up to 22% by weight), though, has allowed to obtain a sufficient interaction between the constituents and, therefore, an exfoliated system [19,20]. The techniques traditionally employed for the evaluation of structure and morphology of nanocomposites are X-ray diffraction and transmission electron microscopy (TEM), sometimes these methods are coupled extending the observations derived from the former with results obtained from the latter [21].

This work was articulated in two main branches: The influence of clay and additives on polymer crystallization was investigated, and the interaction between polymer and clay was evaluated. Wide angle X-ray diffraction (WAXD) was employed to study the polymer matrix, particularly its polymorphism. WAXD, small angle X-ray scattering (SAXS) and TEM were used to investigate the clay behavior.

The purpose of this paper was to clarify the influence on polymer–clay nanocomposite systems of such parameters as processing conditions, molecular weight of the polymer, additives, in order to identify the best conditions to obtain nanocomposites characterized by satisfying mechanical properties.

2. Experimental

2.1. Samples and sample preparation

Two commercially available grades of homopolymer produced by Basell Polyolefins SpA were used in this work. The first is Moplen HP 500J, which is suitable for injection moulding and extrusion applications; it exhibits an excellent stiffness in addition to good processability. The melt flow rate is 3.2 g/10 min (corresponding to a $M_w = 390{,}000$), the flexural modulus is 1500 MPa. The second one is Moplen HP 500N which is suitable for injection moulding applications too; the melt flow rate for this grade is 12 g/10 min (corresponding to a $M_w = 250{,}000$) the flexural modulus is around 1550 MPa.

The synthetic clay used for this work was Cloisite 15-A produced by Southern clay products. Cloisite 15-A is montmorillonite ion-exchanged with octadecylammonium ions. Two different agents were added to the polymer: The first one was a polymer based on maleated polypropylene (PP-MA) containing approximately 0.7 wt% of grafted maleic anhydride usually used as compatibilizing agent, the second one was a processing aid agent, Abriflo 65 (Abril Industrial Waxes Ltd), based on monoethanolstereamide usually employed as a specialized low melting point wax for thermoplastic films.

The components were mixed in a reciprocating single screw extruder, Buss MDK 70. The machine setup can be adjusted in order to change the mixing energy to the final product and to allow component feeding into different feeding ports. For instance, it was possible to feed the clay both in the main (before polymer melting) and in the second feeding port (after polymer melting).

The profile of the employed screw introduced a further differentiation of the samples: the A profile is that normally used for talc filled grades, the B profile is characterized by the elimination of restriction rings and in the C profile reverse kneading elements were inserted to increase distributive mixing and residence time. A total of 18 samples were examined.

The first letter in the designation of the samples indicates the type of screw profile used (A, B or C), the second letter is related to the molecular weight of the polymer matrix ($L = 12$ MFR, and $H = 3.2$ MFR), the third letter identifies the additive (a = Abriflo or k = PP-MA) and the last figure designates the feeding port chosen for the addition of the clay. Table 1 shows the characterization data relative to all the examined samples.

The pellets obtained were subsequently processed both by injection moulding and compression moulding.

Injection-moulded specimens were prepared in accordance with ISO 294-1 or ISO 294-3.

Test specimens were conditioned in accordance with ISO 291 for at least 40 h at (23 ± 2)°C and (50 ± 5)% relative humidity.

Compression moulded specimens were prepared by homogenization of the pellets in a camera-mix and subsequent moulding in a 12×12 cm^2 die with a hot press (with a thickness of 2 or 3 mm). The plates obtained were then cooled under a cold press, still under pressure.

The operational conditions where the followings:

T oil camera mix = 200 °C.
T hot plate = 200 °C.
P hot plate = 180–200 bar.
T cold plate = room temperature.
P cold plate = 50 bar ca.
Time in camera mix = 5 min.

Table 1
Characterization of the examined samples

Sample	MFR (g/10 min)	Screw setting	Additive	Feeding port	Flexural modulus (N/mm^2)	Yield stress (N/mm^2)	HDT (°C)
HP500J	3.2	–	–	–	1500	34.0	85
HP500N	12	–	–	–	1550	35.0	80
AHa1	4.4	A	Abriflo	Main	2023	46.0	103
AHa2	4.6	A	Abriflo	Melt	2100	35.3	102
AHk1	4.6	A	PP-MA	Main	1970	37.7	110
AHk2	4.6	A	PP-MA	Melt	1820	37.1	113
ALa2	15.4	A	Abriflo	Melt	2241	35.7	106
ALk2	10.9	A	PP-MA	Melt	2240	38.8	120
BHa1	4	B	Abriflo	Main	2015	35.6	103
BHa2	4.5	B	Abriflo	Melt	2090	35.9	105
BHk1	3.8	B	PP-MA	Main	2069	38.3	112
BHk2	4	B	PP-MA	Melt	1836	37.3	115
BLa2	14.8	B	Abriflo	Melt	2224	36.0	111
BLk2	–	B	PP-MA	Melt	2330	39.7	119
CHa1	4.4	C	Abriflo	Main	2040	35.3	105
CHa2	–	C	Abriflo	Melt	2096	35.3	102
CHk1	4.4	C	PP-MA	Main	2029	38.0	114
CHk2	4.2	C	PP-MA	Melt	1830	37.8	114
CLa2	15.3	C	Abriflo	Melt	2181	35.6	110
CLk2	10	C	PP-MA	Melt	2243	38.8	117

MFR, melt flow rate; HDT, heat deflection temperature.

2.2. Mechanical properties

The flexural and elongational properties were determined in accordance with ISO 178 using an Instron 4301 instrument on the injection-moulded specimens. Heat deflection temperature (HDT), which is a measurement of the temperature at which an arbitrary deformation occurs, was evaluated with a CEAST HDT 6 placing the specimen in an oil bath under a load of 460 kPa (ISO 75). The melt flow rate (MFR) was measured by forcing the melt through a capillary under a dead load at constant temperature (2.16 kg, 230 °C in accordance with ASTM D1238).

In Table 1 the most relevant results obtained from the physico–mechanical analyses of the polymer–clay nanocomposites are reported. For simplicity we will refer only to the most representative characteristics like flexural modulus (MEF), yield stress, HDT and MFR. For comparison the data related to the two homopolymers used as matrix are also reported.

For what concern the MEF it can be seen how the presence of 5% of organo-clay has brought to an increases of 50% in comparison to the unfilled polymer.

Consistent improvements are also visible for the HDT and in many cases also for the yield stress.

The MFR values show a slight increase except for the ALk2 and CLk2 samples that, with BLk2, are among the most property-enhanced.

2.3. WAXD

Transmission patterns were recorded in the diffraction range 5–40° 2θ by a diffractometer GD 2000 (Ital Structures) working in a Seeman–Bohlin geometry and with a quartz crystal monochromator on the primary beam (Cu $K_{\alpha 1}$ radiation). Reflection patterns were recorded by a Philips X'Pert PRO diffractometer equipped with a graphite monochromator on the diffracted beam (Cu K_{α} radiation). The angular range for the measurements in the reflection geometry was 1.5–40° 2θ.

A least-square fit procedure was applied according to Hindeleh and Johnson [22] to reproduce WAXD profiles. The relative amount of the β-form was calculated according to Turner Jones [23].

2.4. SAXS

The SAXS patterns of the samples were recorded by an MBraun system, utilizing a Cu K_{α} radiation from a Philips PW 1830 X-ray generator. The data were collected by a position sensitive detector, in the scattering angular range 0.1–5.0° 2θ and they were successively corrected for blank scattering.

Finally, the Lorentz correction was applied: $I_1(s) = 4\pi s^2 I(s)$, where $I_1(s)$ is the one-dimensional scattering function and $I(s)$ the desmeared intensity function, being $s = (2/\lambda)\sin\theta$.

2.5. SAXS data analysis

The evaluation of the SAXS patterns according to some theoretical distribution models [24] was carried out referring to the Hosemann model [25], that assumes the presence of lamellar stacks having an infinite side dimension. This assumption takes into account a

monodimensional electron density change along the normal direction to the lamellae.

This method was already extended to describe the hard-soft periodical system in fluorinated elastomeric polyurethanes [26] and, in this study on nanocomposites, it was applied both to the polymeric lamellar stacks and to the alternation of high-density allumino-silicate layers with low-density regions interposed.

The intensity profile was evaluated as:

$$I(s) = I^{\mathrm{I}}(s) + I^{\mathrm{II}}(s)$$

where

$$I^{\mathrm{I}}(s) = \frac{(\rho_Y - \rho_Z)^2}{4\pi^2 s^2 X} \times \frac{|1 - F_Y|^2(1 - |F_Z|^2) + |1 - F_Z|^2(1 - |F_Y|^2)}{(1 - F_Y F_Z)^2}$$

$$I^{\mathrm{II}}(s) = \frac{(\rho_Y - \rho_Z)^2}{2\pi^2 s^2 XN} \mathrm{Re}\left\{\frac{F_Z(1 - F_Y)^2(1 - (F_Y F_Z)^N)}{(1 - F_Y F_Z)^2}\right\}$$

In these equations, F_Y and F_Z represent the Fourier transforms of the distribution functions of the high-density (Y) and of the low-density (Z) regions, ρ_Y and ρ_Z are the electron densities of the high and low-density regions, respectively, N is the number of layers (polymeric lamellae or allumino-silicate layers) in the system and X the average long period. A fitting procedure of the calculated one dimensional scattering functions with the experimental ones allows to optimize the values of the high and low density region thicknesses. Crystallinity (Φ_{SAXS}) was evaluated as the ratio between the thickness of the high density regions over the long period $X = Y + Z$.

2.6. TEM

TEM analysis were performed by a TECNAI 10 FEI. Samples were stained by RuO_4 and cryomicrotomed. Sections about 100 nm thick were obtained and analyzed. Image analysis was performed by the program Analysis SIS 6.0.

3. Results and discussion

3.1. Polymorphism

It is known [23,27] that PP may crystallize in different forms: α, β and γ. Polymorphism is important for technological reasons, because each phase has different physical and mechanical characteristics, so it is of the utmost importance to determine how the material crystallizes in presence of additives like nanofillers and whether these crystallographic forms are homogeneous.

Two different geometries were used to collect WAXD patterns: transmission diffractograms allowed the investigation of the crystallization of the whole matter forming the samples, while reflection geometry gave useful information about samples' surface.

While the mixing dynamics, related to the screw profile or the feeding port through which the clay was added, and the PP molecular weight were not found in this work to have a significant role in determining polymorphism, differences in WAXD profiles were originated when a different additive, either a maleated polypropylene polymer (PP-MA) or monoethanolstereammide (Abriflo), were used. Samples with PP-MA agent showed a complete β-crystallization in reflection patterns, while 100% α-form was exhibited in transmissions profiles. The occurrence of β-phase on the surface of the samples additivated with PP-MA, was probably due to the shear–stress resulting from processing conditions [27].

Samples produced with Abriflo showed a different behavior. No significant difference in polymorphism was detected between transmission and reflection profiles and a mixed phase α + β was always observed. In all this kind of samples, the relative amount of β-phase never exceeded 30% for both geometries, denoting a rather uniform crystallization in the bulk and in the samples' surface. The constant presence of β-form in all the matter forming these specimens may be attributed to the processing aid agent, which could act as nucleating agent for β-phase. Stearic-acid derivatives are known as useful promoters of this particular crystallographic phase [28–30].

3.2. SAXS analysis of lamellar morphology

Through reconstruction of SAXS signals, the lamellar morphology of the polymer was studied focusing on four samples: AHa1, AHa2, ALk2 and BLk2. These particular samples were selected to estimate the influence on lamellar organization of polymer molecular weight and clay dispersion. ALk2 and BLk2, characterized by a partial clay exfoliation, were compared to AHa1 and AHa2, that show only intercalation (vide infra). The model yielding the best fitting was based on a single population of lamellae with a variable thickness of the crystalline layers. The models assuming a double population gave unacceptable results, so it can be concluded that the molecules crystallized in the α and β phase are organized in similar lamellar stacks. It may be inferred, then, that in the same lamella, polypropylene chains can order themselves either in α and β phase [31]. One of the fittings is shown in Fig. 1 and in Table 2 the best parameters resulting from fitting procedure are presented.

It can be seen that the crystallinities assessed by SAXS have larger values relative to those estimated by WAXD. This divergence can be explained considering the difference between the two techniques. WAXD allows the detection of all the crystalline forms in the sample, while SAXS is only

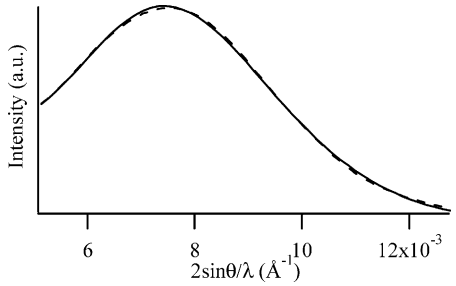

Fig. 1. Fit (solid line) of the SAXS pattern (dashed line) of sample ALk2.

sensitive to the crystalline regions organized in lamellar stacks.

Anyways, it can be concluded that for the considered samples, the morphology of lamellar stacks is practically unaffected by the molecular weight of the polymer, the additive or by the processing conditions chosen for the preparation of nanocomposites. It is not surprising that the lamellar stacks are not affected by the clay dispersion, because it is known [16] that clay particles have a tendency to diffuse out of the interlamellar region.

3.3. Polymer–clay interaction

In Figs. 2 and 3, WAXD patterns of the samples are compared to the profile of cloisite 15-A. Pure organoclay shows in this range a (001) basal signal at 2.8° 2θ, that is associated to the stacking of the clay sheets. The corresponding d_{001} is related to the periodicity of these layers, that are, therefore, 31.5 Å distant one from another. In nanocomposites, a shift of this peak toward small angles would be associated with intercalation, while its disappearance would be a sign that exfoliation has occurred. In order to correctly assess the degree of interaction between polymer and clay, WAXD and SAXS should be used complementarily. Disappearance of a basal peak in a WAXD diffractogram alone should not be intended as a clear sign of exfoliation, unless it is supported by SAXS. Extensive intercalation could in fact separate clay layers to such an extent to be undetectable by WAXD but can still be determined by SAXS. Only the disappearance of SAXS signals and TEM observations can confirm that exfoliation has occurred.

Observing the shape and the position of signals clear differences can be seen between samples processed with different agents.

k-Samples, produced with PP-MA (Fig. 2) show a unique

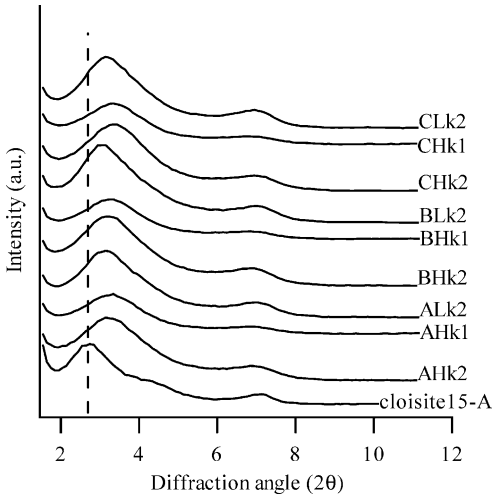

Fig. 2. WAXD patterns of k-samples, compatibilized with PP-MA, compared with pure cloisite. The dashed vertical line corresponds to the periodicity of pure cloisite.

(001) peak around 3.1° 2θ, whereas samples with Abriflo (Fig. 3) exhibit many signals in the region comprised between 2.5 and 10.3° 2θ. These profiles indicate that in k-samples clay sheets did not intercalate, but are still stacked in tactoids. Moreover, the maximum of the (001) peak for these nanocomposites is shifted to wider angles, indicating that clay layers are closer than in pure cloisite 15-A.

This smaller basal-spacing with respect to cloisite indicates that a collapse in the clay sheets has taken place. This behavior may be induced by the thermal or mechanical treatments involved in the preparation of the nanocomposites, which probably causes the displacement of ammonium compounds usually present between clay sheets [32]. It has in fact been reported [33] that the ammonium salts used in organoclays are quite thermally unstable. In order to further confirm this hypothesis, simulations were performed of the thermal history that cloisite experienced during the preparation of the nanocomposite. WAXD spectra were taken of montmorillonite at room temperature and at 200 and 230 °C. A significant shift toward wider angles of the (001) basal signals was clearly observed.

Samples with Abriflo exhibit a different behavior (Fig. 3). The peak at around 2.7° 2θ appears at about the same position with respect to the (001) signal by cloisite 15-A. This fact demonstrates the presence of layers organized in small tactoids with no penetration whatsoever of polypropylene molecules. The presence of another peak, not completely observable through WAXD, is suggested by

Table 2
Lamellar (Y) and amorphous (Z) average thicknesses, long period (X), degree of crystallinity measured by SAXS and WAXD (Φ_{SAXS} and Φ_{WAXD}, respectively)

	Y (Å)	Z (Å)	X (Å)	Φ_{SAXS}	Φ_{WAXD}
AHa1	101	32	133	76	52
AHa2	103	34	137	76	47
ALk2	106	25	131	81	57
BLk2	107	22	129	83	49

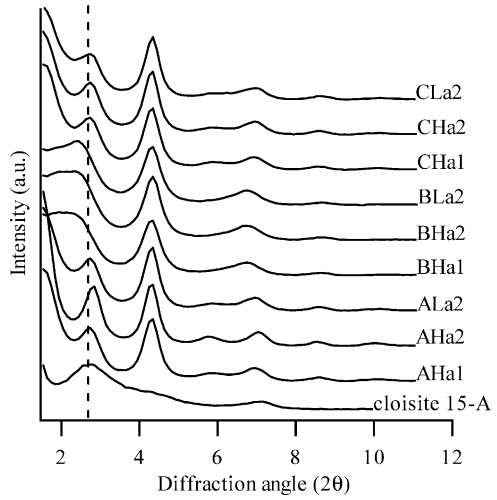

Fig. 3. WAXD patterns of a-samples, processed with Abriflo, compared with pure cloisite. The dashed vertical line corresponds to the periodicity of pure cloisite.

the increasing intensity at very small angles. SAXS analysis confirmed this hypothesis. In Fig. 4 the SAXS profiles of some a-samples are shown. As can be seen, an additional and intense peak associated to a *d*-spacing of 60 Å is evident. This signal can be connected to an intercalated phase where clay sheets are more separated than in cloisite 15-A. In this case polymer chains penetrate into the galleries between adjacent layers expanding the structures and doubling the interlayer distance from 30 to 60 Å.

In addition, the (001) peak produced by the clay stacks which remain 'immiscible' with the polymer is still observable at about 31 Å and, therefore, clearly indicates the existence of two distinct degrees of interaction: in some layers intercalation of polymer chains occurs, whereas others remain stacked in small tactoids without any polymer penetration. The SAXS profiles of the samples compatibilized with PP-MA did not yield further information about the clay structures: these patterns show just one (001) peak, moved to slightly lower *d*-spacing values with respect to pure cloisite, confirming the presence of collapsed clay stacks.

In Fig. 5, SAXS patterns of samples produced with different screw profile are shown.

Comparing the WAXD and SAXS profiles (Figs. 3 and 5), the A and C screw settings yield very similar results, whereas when the B setting is used a different situation is observed. For B samples, the signal corresponding to the intercalated clay is shifted toward wider angles, while on the contrary the layers of the cloisite that has not interacted with the polymer are slightly more distant than in the pure organoclay. In B samples, therefore, the clay is characterized by a very broad signal that spans *d*-spacings from 30 to 60 Å. This shift suggests how, using the B screw setting and thus eliminating the restriction rings, 'platelet compaction' is actually avoided and the interaction between clay and polymer is favored.

A and C screws imply longer extrusion times, that may favor the possibility for clay layers of interacting and recompacting into tactoids, as shown by the sharper peaks in the SAXS diffractogram.

Another important factor that influences the interaction between the components is the polymer average molecular weight [34–37]. Comparing the SAXS patterns of BHk2 and BLk2 (Fig. 6), which differ just for polymer molecular weight, it can be noticed how the (001) peak shifts to lower angles as the molecular weight diminishes.

This behavior was observed both in SAXS and in WAXD profiles, and is due to the fact that short polymer chains facilitate interaction with clay, since penetration into interlayer galleries could be promoted. In other words, the diffusivity of the macromolecular chains in the silicate layers is larger for low molecular weight polymers [34]. TEM analyses confirmed these results. A micrograph of BLk2 is displayed in Fig. 7. Exfoliated clay layers are visible, along with tactoids. Inside the same tactoid, some of the layers are characterized by a stacking very similar to that of pure cloisite, some others are more spaced, indicating that intercalation of the polymer has occurred. The single delaminated layers could not be revealed by SAXS because of their structural disorder that does not have any periodicity.

In this case, clay seems to be homogeneously dispersed in polymer matrix and even oriented along a preferential direction: Diagonally from left to right along the injection direction of the sample. AHk1 (Fig. 8) shows less exfoliation phenomena and clay layers remain stacked in collapsed tactoids, inhomogeneously dispersed in the polymer matrix.

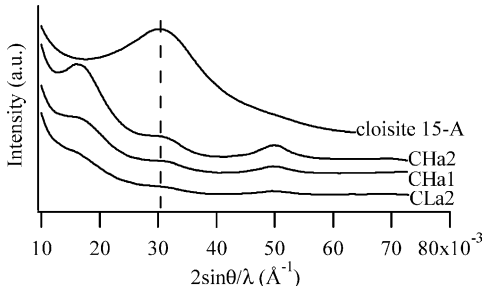

Fig. 4. SAXS patterns of some a-samples compared with pure cloisite. The dashed vertical line corresponds to the periodicity of pure cloisite.

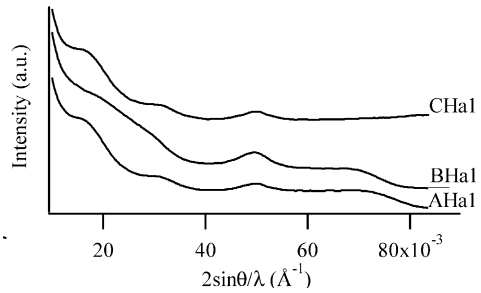

Fig. 5. SAXS patterns of samples produced with different extruder setting.

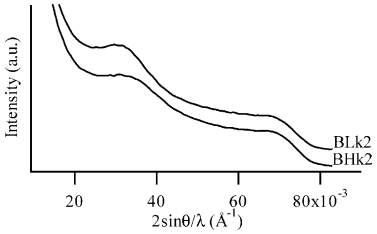

Fig. 6. SAXS patterns of samples BHk2 and BLk2.

In sample AHk1, moreover, very large clay particles were observed, proving the ineffective fragmentation of the filler.

Comparing BLk2 and AHk1, it is confirmed that the best combination of factors for avoiding filler compaction and obtaining a good dispersion of the clay is using a low molecular weight polymer, compatibilized with PP-MA in an extruder equipped with a B-type screw.

A further factor that could influence polymer–clay interaction is the choice of the feeding port in the extrusion procedure. In the production of nanocomposites, in fact, mixing of the components is crucial for a satisfying interaction between polymer and filler.

It may be expected, then, that if the filler is added at an earlier or later stage of the extrusion process, some differences should be noted. Fig. 9 compares SAXS patterns of two a-samples which differ for the feeding port chosen for the introduction of the clay: if it is added through the second feeding port, i.e. to the molten polymer, the (001) signals appear more intense than the peaks produced by the samples where the clay was fed through the main port.

A more intense and sharp peak indicates the presence of structures with a larger number of narrowly distributed layers. A similar situation is observed comparing the samples compatibilized with PP-MA in Fig. 10: the choice of the main port produces a broader peak, almost a shoulder, shifted toward small angles, indicating a much larger distribution in the spacing of the layers in clay particles and therefore, an expansion of the sheets. The residence time in the extruder should, therefore, be accurately calibrated as a function of the type of additive.

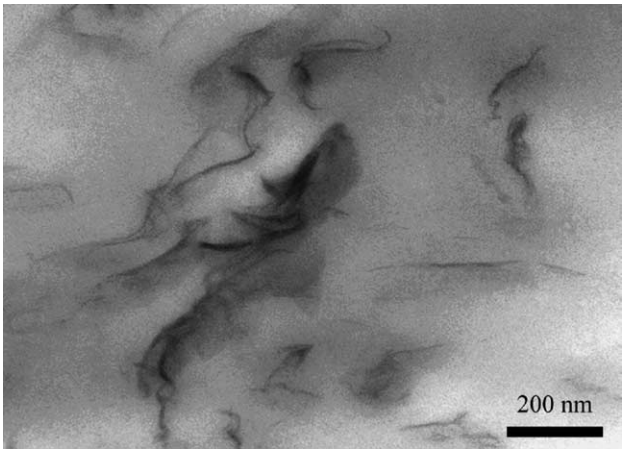

Fig. 7. TEM micrograph of sample BLk2. The scale corresponds to 200 nm.

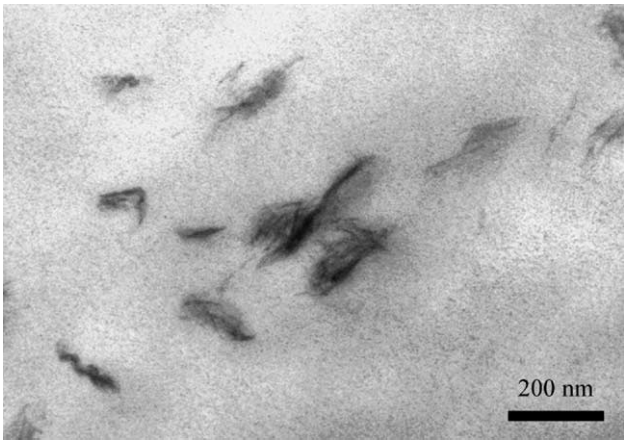

Fig. 8. TEM micrograph of sample AHk1. The scale corresponds to 200 nm.

Figs. 11 and 12 display how tactoids are formed by more layers in AHa2 rather than in AHa1 confirming the differences emerged from XRD analysis. In this case, in fact, feeding the clay in the second port does not allow for enough time to reach an acceptable breaking-up of the stacks.

As can be seen in Figs. 13 and 14, the tactoids in AHa1 show intercalated layers, with a broader distribution in the spacing of the clay sheets, with respect to AHa2.

If the corresponding SAXS traces are examined (Fig. 9), it can be seen that AHa2 produces a rather neat peak in correspondence of pure cloisite, while in AHa1 this signal is broader, showing the coexistence of unaltered, expanded and intercalated clay layers in this latter composite. In both cases no significant exfoliation is exhibited and an uneven filler distribution in the polymer matrix is shown; both these facts are caused by the processing aid agent Abriflo which allows an intercalation by the polymer chains but does not favor an exfoliated structure.

The reason why with Abriflo no exfoliation is observed is to be sought in its mechanism of action. Monoethanolstearammide (Abriflo) is a processing aid agent intended to favor the flow of the polymer chains one with respect to the others and inside the clay layers. Addition of PP-MA is not aimed at improving the mobility of chains, but the affinity of the

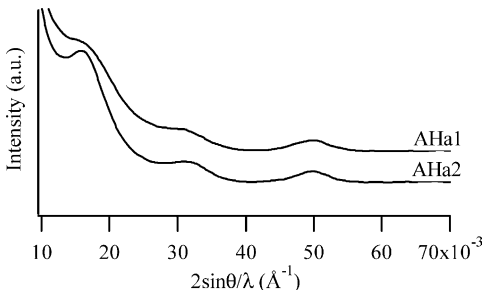

Fig. 9. SAXS patterns of samples AHa1 and AHa2.

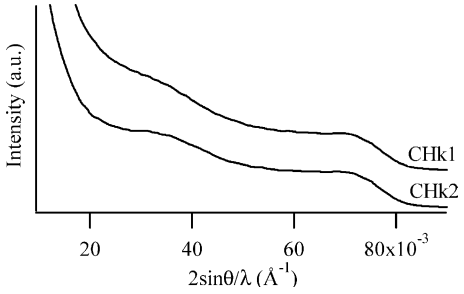

Fig. 10. SAXS patterns of samples CHk1 and CHk2.

polymer with clay layers. While with the processing aid agent mobile macromolecules can enter the montmorillonite sheets but, if allowed the necessary time, may even diffuse out, if PP-MA is employed the polymer–clay interaction is driven by polar affinity and is less likely to be reversible.

3.4. TEM image analysis

Exfoliation, as well as intercalation, leads to an apparent increase of the particles' dimensions. However, a larger particle dimension can arise either from exfoliation/intercalation or from the presence of larger aggregates or stacks of nanoclay. Therefore, combining the evaluation of the area occupied by nanoclays in samples with the same filler concentration with the next neighbor distribution, a description of the nanoclay dispersion and intercalation/exfoliation can be achieved.

The fraction of the total area occupied by nanoclay is shown in Table 3. It is evident that this quantity is slightly increasing from AHk1 to BLk2, because the volume occupied by nanoclay is larger in the latter thanks to a better opening of the tactoids. The filler covers a very low area in AHa1, where the clay distribution is not homogeneous, however, the fraction of the total area relative to the clay increases in AHa2, mainly because of a poor dispersion of larger aggregates if compared to those found in AHa1.

If the data of Table 3 for AHa1 and AHk1 are compared, it is clear that in AHk1 the tactoids are partially exfoliated/intercaled. Looking at the next neighbor distributions (Fig. 15) it is clear that the distribution is fine and narrow for AHk1 and BLk2, while it is broader and bimodal for AHa1 and AHa2. This indicates that for the latter compounds the dispersion is poor and not homogeneous, i.e. particle distance spreads from the average value.

Comparing samples with a narrow distribution (AHk1 and BLk2) the area occupied by nanoclay allows to infer the best intercalation/exfoliation vs tactoid structure.

Considering the clay particles (both single and stacked layers), the aspect ratio value can be assessed as the ratio between width and thickness of the particle.

In this work, the relative frequency of the particles with different aspect ratio has been estimated (Fig. 16). It turns out that, in the samples with poorer dispersion and not opened tactoids (AHa1 and AHa2), the number of particles with higher aspect ratio is remarkably larger with respect to more intercalated/exfoliated structures (AHk1 and BLk2).

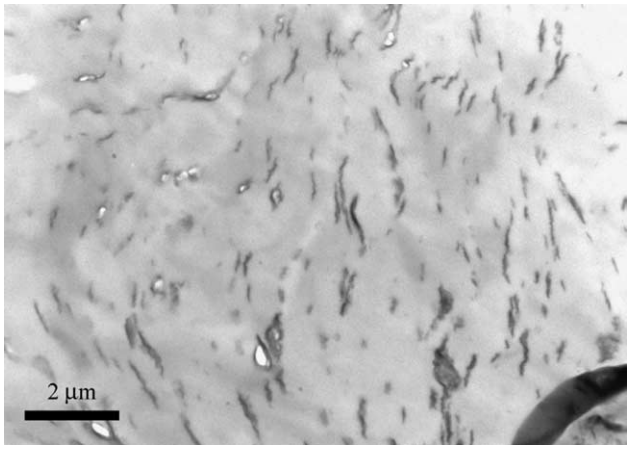

Fig. 11. TEM micrograph of sample AHa1. The scale corresponds to 2 μm.

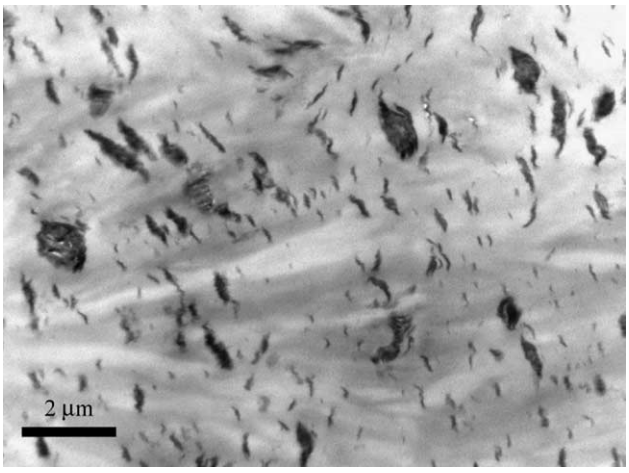

Fig. 12. TEM micrograph of sample AHa2. The scale corresponds to 2 μm.

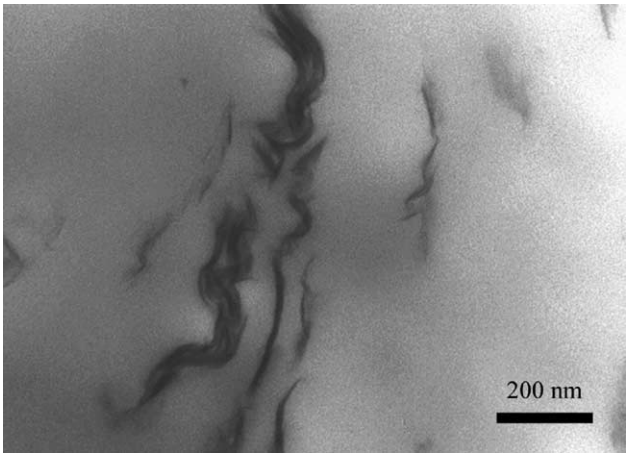

Fig. 13. TEM micrograph of sample AHa1. The scale corresponds to 200 nm.

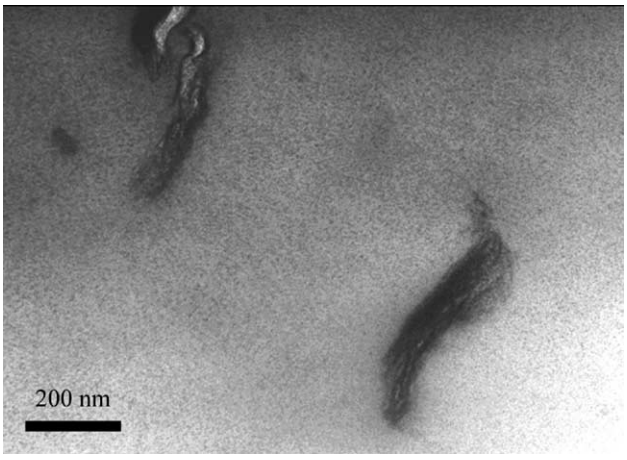

Fig. 14. TEM micrograph of sample AHa2. The scale corresponds to 200 nm.

3.5. SAXS fitting and Scherrer equation

The size of the clay stacks in some nanocomposites was estimated through fitting methods applied to SAXS profiles and through the Scherrer equation applied to WAXD signals.

Two sample were chosen with this aim, AHa1 and AHa2, since they presented different coexisting phases in which the components interact in different ways (Fig. 9).

In the 'intercalated' phase, clay layers allowed polymer chains to penetrate into the van der Waals galleries [4]. These layers produce a SAXS peak at 60 Å. The 'immiscible' phase is made up by platelets remained stacked as in pure cloisite, which origin a SAXS peak at about 31 Å. Both systems may be described by an alternation of high- and low-density regions. The former is due to alumino-silicatic planes that form the clay sheets. The lower density region of the system is composed by anything that is interposed between the layers: ammonium ions, additives and the intercalated polymer.

The fitting procedure reproduced SAXS profiles (Fig. 17), by optimizing the number N of stacked layers, the thickness Z of the low density regions, that indicates how much material is interposed between adjacent clay layers, and the periodicity of the system X, along with the relative standard deviations σ_Z and σ_X. The thickness Y of the alumino-silicatic layers was fixed in 10 Å [7,8,38,39]. These structural parameters are shown in Table 4.

Both for AHa1 and AHa2, going from 'immiscible' to 'intercalated' system, the thickness Z of the region between

Table 3
Fraction of the total area occupied by the clay

Sample	Area occupied (%)
AHk1	6.84
BLk2	7.47
AHa1	4.31
AHa2	7.33

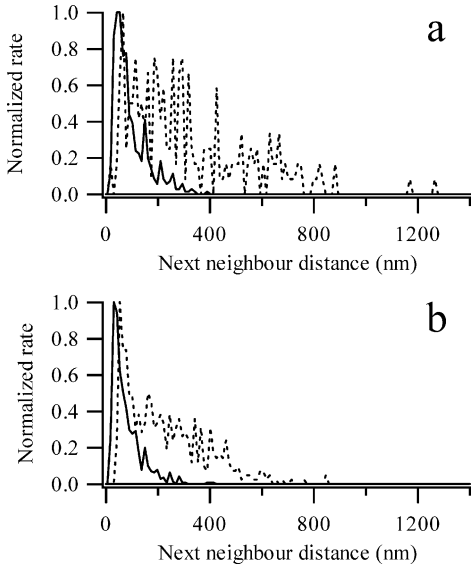

Fig. 15. Next neighbor distributions of nanoclay particles in (a): AHa1 (dashed line) and AHk1 (solid line); (b): AHa2 (dashed line) and BLk2 (solid line). These samples were coupled in order to show the relative differences in the widths of the distributions.

the silicate layers increased from 15 to 39 Å in the case of AHa1 and from 15 to 42 Å in the case of AHa2; this was due to the insertion of polymer chains between the clay sheets. The average number of layers N forming both the intercalated and the immiscible structure was evaluated in about 5 for all the samples, except for the peak corresponding to the intercalated structure of AHa1, where N averaged 4. To confirm the effectiveness of this last method, in describing the main features of clay layers in nanocomposites, Scherrer equation was applied to WAXD (001) signals, associated to the portion of filler, which remained stacked as in pure clay. This equation [40] allows to estimate crystallites' thickness on the basis of the full width at half maximum (β_0) of the corresponding WAXD peaks:

$$L_{hkl} = \frac{0.91\lambda}{\beta_0 \cos\theta}$$

Where L_{hkl} represents the crystallite thickness in a direction perpendicular to that of the crystallographic plane identified by Miller indices hkl, 0.91 is a constant used in the case of

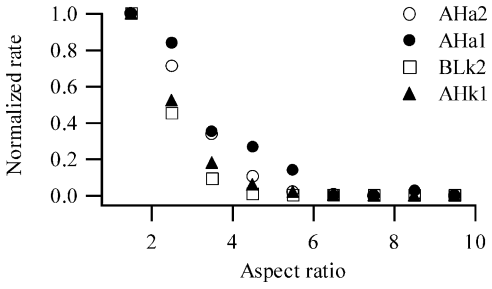

Fig. 16. Aspect ratio distributions of nanoclay particles in AHk1, BLk2, AHa1, AHa2.

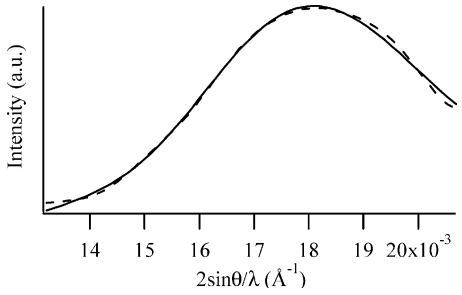

Fig. 17. Fit (solid line) of the SAXS pattern (dashed line) of sample AHa2.

smectites [39], λ the wavelength of the X-radiation and θ the diffraction angle.

Knowing L_{001} values, a further estimation on the number of layers forming 'immiscible' structures can be derived considering that $N = L_{001}/d_{001}$, where d_{001} is the d-spacing associated to the (001) basal signal of cloisite. In Table 4, N values calculated with this relation are shown: they are in good accord with those obtained through the fitting procedure on SAXS signals. For AHa1 four layers were calculated whereas five were obtained for AHa2. TEM micrographs of these samples (Figs. 13 and 14) confirm the presence of aggregates formed by a rather small number of clay layers, compatibly with the results obtained by X-ray diffraction.

SAXS and the Scherrer equation must thus be considered very useful complementary approaches to the study of polymer–clay nanocomposites. When the clay (001) peak is detectable by WAXD, the Scherrer method is the easiest in determining the number of layers that compose the stacks, while the SAXS fitting procedure is useful when intercalation occurred and the clay peaks appear at too small angles for WAXD. Moreover, fitting of SAXS spectra according to the model proposed, yields a number of interesting information related to the thickness and the structure of the clay stacks that cannot be assessed by Scherrer equation.

4. Conclusions

A small effect of the machine/screw setup exists: passing from a multi-purpose screw (A) or one with reversing kneading elements (C) to one with less restriction rings (B), an increase on the properties of nanocomposites is observed.

If smaller and homogeneously distributed clay stacks are sought, the system should be allowed a sufficient residence time to achieve an acceptable breaking up of the layers, so the main feeding port should be chosen for the addition of the clay.

Because the intercalation/exfoliation is a typical diffusive process, a high fluidity of the base resins is preferred: nanocomposites obtained with HP 500N show higher properties enhancements compared to those obtained with HP 500J.

Both maleated PP and monoethanolstereamide can be used to obtain an intercalated nanocomposite but maleated PP is most effective in favoring exfoliation.

Correlation between morphology evaluated by X-ray, TEM and final properties is well defined: the materials produced are in general intercalated nanocomposites with small stacks of organoclay uniformly dispersed in the molten PP. In some cases, a well-intercalated and partially exfoliated structure is obtained and a related properties enhancement can be assigned to this morphological situation. This point opens a consideration concerning the amount of nanofiller to be loaded: provided that we have to improve the exfoliation process, a possible decrease in nanofiller loading (<2 wt%) could avoid the interaction of the exfoliated platelets and the recombination of the clay stacks.

Focusing on the polymer, its crystallization was evaluated through WAXD. A particular attention was dedicated to polymorphism phenomena, which were produced by the presence of substances (monoethanolstereamide) which acted as nucleating agents, or by the processing conditions (shear) which favored the appearance of β polymorphs.

Then, the lamellar morphology of the polymer was studied through SAXS finding that the morphology of the lamellar stacks seems to be unaffected by either the clay dispersion, the molecular weight of the polymer or the different processing settings.

Finally, the dimensions and the composition of the clay stacks were quantified applying a fitting method to the SAXS profiles referred to intercalated and immiscible clay

Table 4
Average number of layers (N), thickness of low density region (Z), periodicity of the layers (X), thickness distribution values (σ_Z/Z and σ_X/X), width at half maximum of WAXD peaks (β_0), crystallites thickness (L_{hkl}) and number of layers evaluated through Scherrer equation ($N_{Scherrer}$)

	N	Z (Å)	X (Å)	σ_Z/Z	σ_X/X	β_0 (2θ)	L_{hkl} (Å)	$N_{Scherrer}$
AHa1 (001) intercalated	4	39	49	0.28	0.23	–	–	–
AHa1 (001) immiscible	5	15	26	0.43	0.30	0.6	131.9	4.1
AHa2 (001) intercalated	5	42	54	0.25	0.20	–	–	–
AHa2 (001) immiscible	5	15	27	0.39	0.28	0.5	166.5	5.3

structures; following this procedure, an estimation of the tactoids' morphology was derived, confirming the obtained results through TEM and the application of Scherrer equation to WAXD signals produced by the same clay stacks.

Acknowledgements

We acknowledge participation in the European Union Network of Excellence Nanofun-Poly. The collaboration of Simona Africano, Gulnaz Idyatullina and Stefano Tortora, researchers at the Basell Poliolefine Italia SpA, Centro Ricerche 'Giulio Natta', was appreciated. The authors also thank J. Rosenthal for the precious discussion on the employment of Abriflo. V.C. gratefully acknowledges financial support by Basell Italia SpA, through a Federchimica grant.

References

[1] Giannelis EP. Adv Mater 1996;8:29.
[2] Sherman LM. Plast Technol 1999;45(6):52.
[3] Ginzburg VV, Singh C, Balazs AC. Macromolecules 2000;33:1089.
[4] Alexandre M, Dubois P. Mater Sci Eng 2000;28:1.
[5] Zanetti M, Lomakin S, Camino G. Macromol Mater Eng 2000;279:1.
[6] Vaia RA, Wagner HD. Mater Today 2004;7(11):32.
[7] Ray SS, Okamoto M. Prog Polym Sci 2003;28:1539.
[8] Shao W, Wang Q, Ma H. Polym Int 2005;54:336.
[9] Brune DA, Bicerano J. Polymer 2002;43:369.
[10] Luo JJ, Daniel IM. Compos Sci Technol 2003;63:1607.
[11] Fornes TD, Paul DR. Polymer 2003;44:4993.
[12] Hasegawa N, Okamoto H, Kato M, Tsukigase A, Usuki A. Macromol Mater Eng 2000;76:280.
[13] Hasegawa N, Okamoto H, Kato M, Usuki A. J Appl Polym Sci 2000; 78:1981.
[14] Nam PH, Maiti P, Okamoto M, Kotaka T, Hasegawa N, Usuki A. Polymer 2001;42:9633.
[15] Okamoto M, Nam PH, Maiti P, Kotaka T, Hasegawa N, Usuki A. Nano Lett 2001;1:295.
[16] Maiti P, Nam PH, Okamoto M, Kotaka T, Hasegawa N, Usuki A. Polym Eng Sci 2002;42:1864.
[17] Okamoto M, Nam PH, Maiti P, Kotaka T, Nakayama T, Takada M, et al. Nano Lett 2001;1:503.
[18] Reichert P, Nitz H, Klinke S, Brandsch R, Thomann R, Mülhaupt R. Macromol Mater Eng 2000;275:8.
[19] Kawasumi M, Hasegawa N, Kato M, Usuki A, Okada A. Macromolecules 1997;30:6333.
[20] Hasegawa N, Kawasumi M, Kato M, Usuki A, Okada A. J Appl Polym Sci 1998;67:87.
[21] Giannelis EP, Krishnamoorti R, Manias E. Adv Polym Sci 1999;138: 107.
[22] Hindeleh AM, Johnson DJ. J Phys D: Appl Phys 1971;4:259.
[23] Turner-Jones A, Aizlewood JM, Beckett DR. Makromol Chem 1964; 75:134.
[24] Marega C, Marigo A, Cingano G, Zannetti R, Paganetto G. Polymer 1996;37:5549.
[25] Hosemann R, Bagchi SN. Direct analysis of diffraction by matter. Amsterdam: North Holland; 1962.
[26] Tonelli C, Ajroldi G, Marigo A, Marega C. Polymer 2001;42:9705.
[27] Moore EP. Polypropylene handbook. Cincinnati: Hanser; 1996.
[28] Shi G, Zhang X, Qiu Z. Makromol Chem 1992;193:583.
[29] Shi G, Zhang X, Cao Y, Hong J. Makromol Chem 1993;194:269.
[30] Filho DS, Oliveira CMF. Makromol Chem 1993;194:279.
[31] Marigo A, Marega C, Causin V, Ferrari P. J Appl Polym Sci 2004;91: 1008.
[32] Pozsgay A, Frater T, Papp L, Sajo I, Pukanszky B. J Macromol Sci, Part B 2002;B41:1249.
[33] Gao F. Mater Today 2004;7(11):50.
[34] Vaia RA, Jandt KD, Kramer EJ, Giannelis EP. Macromolecules 1995; 28:8080.
[35] Vaia RA, Giannelis EP. Macromolecules 1997;30:7990.
[36] Koo CM, Ham HT, Kim SO, Wang KH, Chung IJ, Kim D, et al. Macromolecules 2002;35:5116.
[37] Lyatskaya Y, Balazs AC. Macromolecules 1998;31:6676.
[38] Brown G. The X-ray identification and crystal structures of clay minerals. London: Mineralogical Society; 1961.
[39] Brindley GW, Brown G. Crystal structures of clay minerals and their X-ray identification. London: Mineralogical Society; 1980.
[40] Klug HP, Alexander LE. X-ray diffraction procedures. New York: Wiley; 1974.